

Addressing the symmetry of a converging cylindrical shock wave in water close to implosion

Cite as: Appl. Phys. Lett. **118**, 174103 (2021); doi: [10.1063/5.0050033](https://doi.org/10.1063/5.0050033)

Submitted: 11 March 2021 · Accepted: 18 April 2021 ·

Published Online: 30 April 2021





View Online



Export Citation



CrossMark

A. Rososhek,^{a)}  D. Nouzman, and Ya. E. Krasik 

AFFILIATIONS

Physics Department, Technion, Haifa 3200003, Israel

^{a)} Author to whom correspondence should be addressed: sasharos@campus.technion.ac.il

ABSTRACT

We report experimental and numerical results relevant to the dynamics in the vicinity of the implosion axis of a strong shock wave generated by an underwater electrical explosion of a cylindrical array. Experiments were conducted using both sub-microsecond and microsecond timescale pulsed generators with stored energy up to ~ 5 kJ, delivering $\sim 420/350$ kA with a 320/1000 ns rise time pulses to the array, respectively. The backlighted images of the converging shock wave and the light emission around the cylindrical axis indicate strongly that the shock wave front keeps its azimuthal uniformity as far as $r \approx 30 \mu\text{m}$. Also, images obtained almost simultaneously with the implosion suggest symmetric convergence < 2 ns prior to the shockwave's arrival to the axis. In addition, the light emission obtained by a photo-multiplying tube suggests the existence of a ~ 200 ns long, almost constant, strong afterglow immediately following the light emission peak related to the implosion.

Published under an exclusive license by AIP Publishing. <https://doi.org/10.1063/5.0050033>

The physics of high energy density (HED) and warm dense matter (WDM)¹ attracts considerable attention due to their importance for planetary science and astrophysics, inertial confinement fusion, and validation of equations of state (EOS) along with conductivity models. Recent research of the underwater electrical explosion of wires and wire arrays showed that this approach can be applied for HED and WDM studies using moderate-pulsed power generators.² It was shown that an underwater electrical explosion of spherical/cylindrical wire arrays results in the generation of a strong shock wave (SSW), the convergence of which can lead to extreme parameters of the water in the vicinity of the implosion axis/origin if the SSW keeps its symmetry.³ While theoretical and simplified numerical simulations predicted that an unconstrained pressure spike appears on the SSW's convergence axis/origin,^{3,4} how far can symmetry hold, or in other words, how extreme one can get, is an open key question. In a recent paper,⁵ in an underwater electrical explosion of cylindrical wire arrays, a pressure exceeding 10^{11} Pa was estimated as the SSW approached $r < 10 \mu\text{m}$. The results of Yanuka *et al.*,⁶ employing a small pulse generator with the stored energy of < 500 J, showed that the cylindrical SSW self-repairs initial azimuthal non-symmetries and symmetry holds down to $r \approx 30 \mu\text{m}$.

The question of the stability of the cylindrical shock wave over the last few micrometers of the convergence is currently open because of considerable difficulties with the experimental optical diagnostics.

The latter is related to the front smearing due to shock high velocity and finite time of the frame exposure, the shock is likely to become radiative, and optical alignment becomes a crucial issue and challenges with time synchronization. The results of two-dimensional modeling⁷ coupled with EOS⁸ for water with artificially introduced corrugation instability at a shock radius of 0.2 mm did not show the development of instability because the shock front self-repaired. Also, the linear theory⁹ that considers quasi-stationary shock wave predicts corrugate instability with an increment on a microsecond timescale.

In the present research, we study the dynamics of the imploding SSW generated by an underwater electrical explosion of cylindrical Cu wire arrays in the kJ range of the energy deposited into the array. We use two different generators with the stored energy of ~ 5 kJ operating on sub- μs and μs -timescales. For both, the parameters of the wire arrays were adjusted, so that the discharge was almost critically damped generating the fastest SSW¹⁰ with the most efficient energy and energy rate transfer from the exploding wires into the water flow. In this research, we focus on measurements of the SSW parameters at radii closest to the implosion axis and on time-resolved light emission from the water at $r < 0.5$ mm. The results are compared with one-¹¹ (1D) and two-dimensional⁷ (2D) hydrodynamic simulations (HDs) coupled with the EOS⁸ for water and copper. The results of these simulations are used to estimate the thermodynamic parameters of water in the vicinity ($r < 10 \mu\text{m}$) of the implosion axis, where measurements

are challenging because of the demand of sub-ns-time and μm -space resolution. In these simulations, we use the measured energy deposited into the wires as an input parameter, while the efficiency of the energy transfer into the internal energy of the exploding wires is used as a fitting parameter, which is adjusted, so that the simulated SSW's time-of-flight (TOF) is almost equal to that measured.

The research was conducted on a μs -timescale generator¹² (Gen1) with $\sim 5\text{ kJ}$ stored energy, which produces a current pulse of $\sim 380\text{ kA}$ amplitude with $\sim 1.2\ \mu\text{s}$ rise time on an $\sim 18\text{ nH}$ inductive load. For sub- μs -timescale studies, we used a generator¹³ (Gen2) with $\sim 5\text{ kJ}$ stored energy, supplying $\sim 480\text{ kA}$ with $\sim 450\text{ ns}$ rise time on an $\sim 18\text{ nH}$ inductive load. 40 wires, 40 mm long, $114\ \mu\text{m}$ diameter each, 10 mm and 20 mm diameter cylindrical Cu wire arrays were used in experiments using Gen1. For Gen2 experiments, we used 10 mm diameter arrays consisted of 60 wires each of $80\ \mu\text{m}$ diameter and 40 mm length.

The experimental setup using Gen1 is shown in Fig. 1. A single-mode continuous-wave laser (2.7 W, 532 nm) coupled to a single-mode fiber was used to backlight the SSW. Shadow images of the SSW were captured by an intensified charge-coupled device (ICCD) XXRapidFrame fast-framing camera (Stanford Computer Optics). The microscope optical system was built employing 150 mm and 750 mm focus lenses, and an objective inside the ICCD XXRapidFrame camera to obtain a sharp focus at the mid-height of the array on each of four cameras photocathode. The pixel size was $\sim 1.7\ \mu\text{m}$ and $\sim 0.8\ \mu\text{m}$ for the setups in the experiments with Gen1 and Gen 2, respectively. A photo-multiplying tube (PMT) Hamamatsu R7400U-04 collected the light emitted from a region of $r < 0.5\text{ mm}$. To prevent saturation of the PMT from the laser light, two notch filters ($532\text{ nm} \pm 10\text{ nm}$) with a total attenuation of $\sim 10^6$ were used (see Fig. 1). The optical system's alignment was performed using two sets of two perpendicularly crossing $20\ \mu\text{m}$ diameter Cu wires, one placed on the high voltage electrode and the second on the ground electrode of the array. The alignment procedure, performed with an additional optical system of $\times 25$ magnification, was completed when the two crosses coincided on the screen. However, the $\sim 60\text{ mm}$ distance between the crosses does not allow sharp focusing, which results in optical distortions estimated to be significant for $r < 50\ \mu\text{m}$.

When using Gen2, the waveforms of the discharge current and voltage were measured using B-dot and D-dot probes, while with Gen1, we used a Rogowski coil and a Tektronix voltage divider. Waveforms of the deposited power and energy, calculated from the

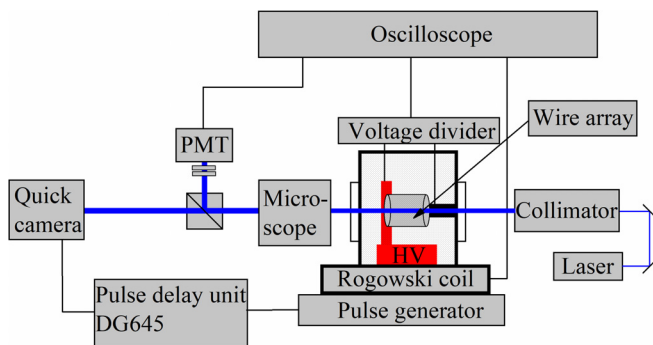


FIG. 1. Experimental setup for the experiments on Gen1.

measured discharge current I_c and the resistive voltage $\phi_R = \phi - LdI_c/dt$, where ϕ is the measured voltage and L is the load inductance, are shown in Fig. 2. One can see that the deposited power rise time for Gen1 and Gen2 is $\sim 1260\text{ ns}$ and $\sim 375\text{ ns}$, respectively. The power/energy deposition rate between the two generators differs by a factor of ~ 3.4 . However, for quasi-spherical arrays explosions (see Ref. 14), the TOF of the SSW, generated for identical conditions, was almost the same. Moreover, for explosions using 10 mm diameter cylindrical wire arrays, the SSWs TOF using Gen2 ($1600 \pm 5\text{ ns}$) and the TOF Gen1 ($1640 \pm 30\text{ ns}$)¹⁵ were almost identical. Here, the SSW TOF was defined as the time delay between the beginning of the light emission spike registered by the PMT and the maximum of the deposited power. Such a close resemblance of TOFs is explained by that for both, similar energy is deposited by the exploding wire array into the water flow, during the period it takes for both SSWs to reach almost identical radii, that is, when the SSWs become self-similar.^{3,4}

In Figs. 3(a)–3(c), we present shadow images (frame exposure time: 2 ns) of the SSW obtained in experiments for the explosion of 20 mm diameter arrays, using Gen1. The time delay between the frames in Figs. 3(a)–3(c) was set to 50 ns, and the observed radii are $\sim 350\ \mu\text{m}$, $\sim 200\ \mu\text{m}$, and $\sim 40\ \mu\text{m}$, respectively. These data allow the calculation of the SSW's average velocity, which is increasing from $\sim 3000\text{ m/s}$ (radii range: $350\text{--}200\ \mu\text{m}$) to $\sim 3300\text{ m/s}$ (radii range: $200\text{--}40\ \mu\text{m}$). One can see that the SSW keeps its azimuthal symmetry in all three frames, although the slight optical distortion stretches the image in the vertical direction.

In Figs. 3(d)–3(f), we present the framing camera images (frame exposure time: 1 ns) of the SSW obtained in experiments for the explosion of 10 mm diameter arrays, using Gen2. The time delay between the images in Figs. 3(d) and 3(e) was 20 ns and 15 ns between Figs. 3(e) and 3(f), respectively. One should note that for Gen2, because of its design, the alignment of the cylindrical array and the optical axis are complicated. For example, an axial misalignment $\sim 10^{-20}$ results in a radial distortion of $\sim 10\ \mu\text{m}$. Taking into account that at larger radii, the SSW front holds its symmetry,^{2,3,6} we assume that the optical distortions seen in the frames seen in Figs. 3(d)–3(f) are the result of this misalignment. Thus, despite these non-symmetric pictures, we analyzed these images using circular sector fitting to estimate the

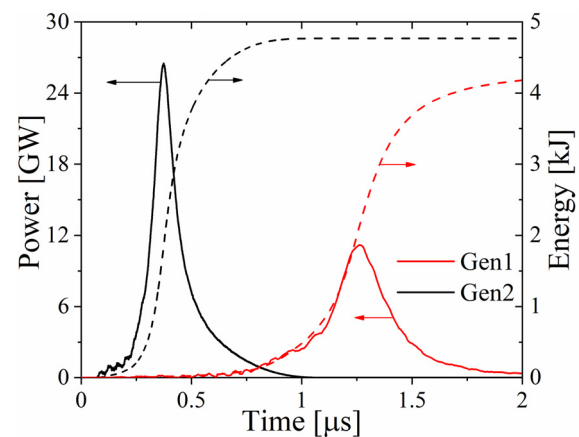


FIG. 2. Waveforms of the deposited power (solid lines) and energy (dashed lines) measured during array explosions using Gen1 (red) and Gen2 (black).

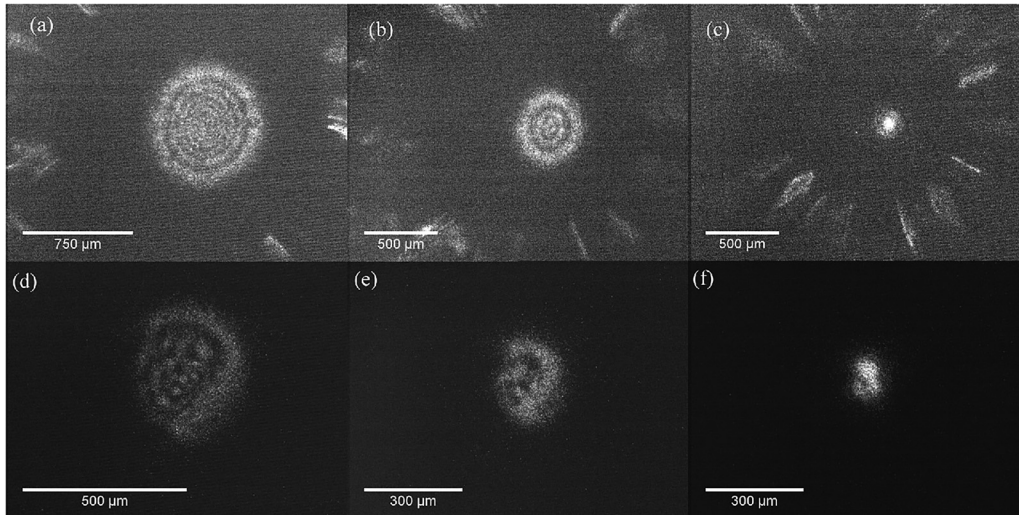


FIG. 3. Shadow framing images of the SSW front, obtained in experiments with Gen1 (a)–(c) and Gen2 (d)–(f) generators.

SSW's radius and velocity. Applying this fit, we obtained the SSW's average velocity, which is increasing from ~ 4000 m/s (radii range: $180\text{--}100\ \mu\text{m}$) to ~ 4800 m/s (radii range: $100\text{--}30\ \mu\text{m}$). Here, let us note that these shock velocities, together with the finite frame exposure times, smear the shock front. Therefore, possible azimuthal non-uniformities with a typical size of $\leq 7\ \mu\text{m}$ for Gen1 at $r = 40\ \mu\text{m}$ (exposure time of 2 ns) and $\leq 5\ \mu\text{m}$ for Gen2 at $r = 30\ \mu\text{m}$ (exposure time of 1 ns) were indistinguishable. The eccentricity $e = \sqrt{1 - (b^2/a^2)}$ of the ellipses seen in Figs. 3(a) and 3(d), where a and b the length of the semi-major and minor axes respectively, is 0.35 ($680/720\ \mu\text{m}$) for Gen1 and 0.45 ($380/340\ \mu\text{m}$) for Gen2. Thus, one can estimate the alignment error of the optical and cylindrical axes as $\alpha = (b - a)/L \approx 0.001^\circ$ for both Gen1 and Gen2, where $L = 40\ \text{mm}$ is the length of the array. In Fig. 4, we present the results of 1D HD modeling for the experiments discussed above. One can see that at $r = 40\ \mu\text{m}$ (Gen 1) and $r = 30\ \mu\text{m}$ (Gen 2), the SSW velocities are 4600 m/s and 6000 m/s, respectively. These

velocities are in satisfactory agreement with the experimentally measured average SSW velocities. Indeed, using a self-similar approximation for the SSW's convergence,³ the SSW's velocity can be estimated as: $D = 2D_{av}(r_1/r_2)^{0.333} [1 + (r_1/r_2)^{0.333}]^{-1}$, which results in 4200 m/s (Gen 1) and 5800 m/s (Gen 2). Thus, assuming SSW convergence symmetry at $r \approx 10\ \mu\text{m}$, the pressure behind the shock front reaches $\sim 20\ \text{GPa}/30\ \text{GPa}$, and the SSW velocity is $\sim 6000\ \text{m/s}/7500\ \text{m/s}$ for Gen1/Gen2, respectively.

In Fig. 5(a), we present a magnified image (200×200 pixels) of the central region seen in Fig. 3(c). To better understand this light pattern, the background was subtracted and a moving average filter was applied. The resulting light intensity distribution in the x and y directions is shown in Fig. 5(b), when x - y grid points represent spatial locations, and the z -axis indicates the normalized intensity. The radius was estimated [see Fig. 5(c)] using the Full-Width-Half Maximum (FWHM) of the integrated along y -direction normalized light

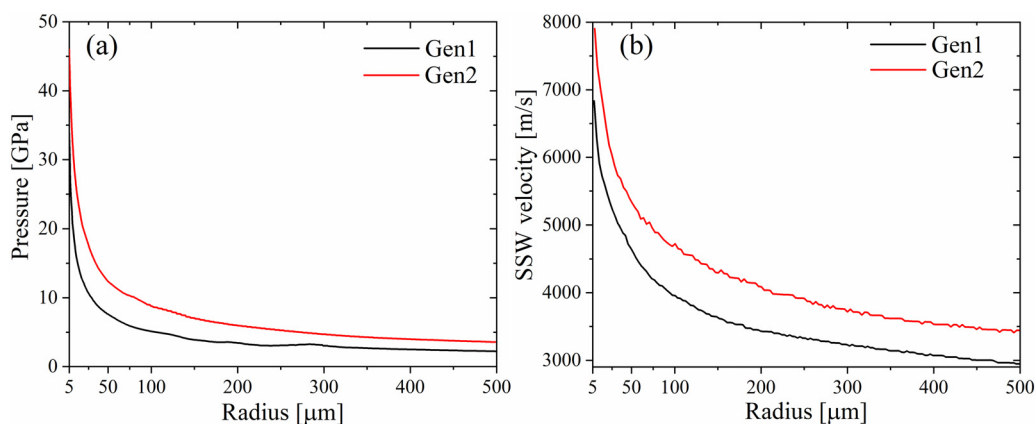


FIG. 4. The pressure behind the SSW front (a) and the SSW velocity (b) obtained from the 1D HD simulation.

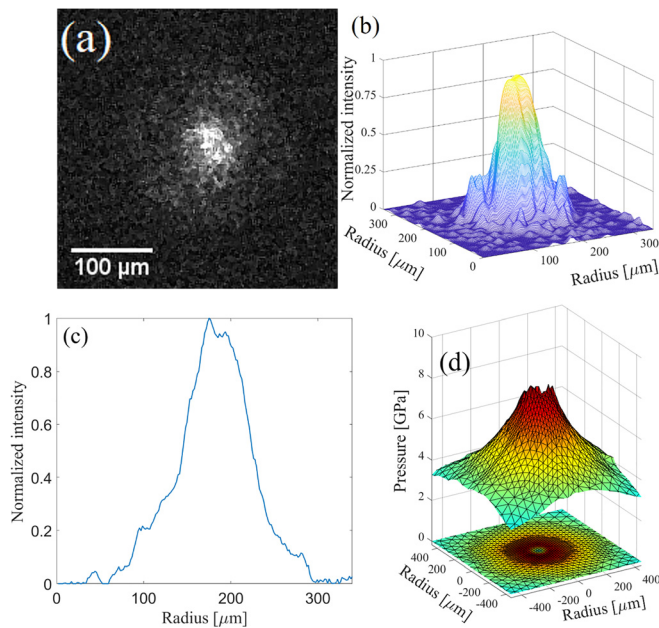


FIG. 5. (a) Magnified image of the central region of Fig. 3(c); (b) 3D noise-filtered plot of the light pattern seen in (a); (c) y -integrated profile of (a); (d) 2D HD simulated pressure distribution when the SSW reached $r \approx 40 \mu\text{m}$.

intensity's dependence. A similar FWHM of the normalized light intensity was obtained when it was integrated along the x -direction. One can see in Fig. 5(c) that the distribution is almost Gaussian (normalized $\chi^2 \approx 0.8$), an indication that the symmetry of the imploding SSW is conserved as far as $r \approx 40 \mu\text{m}$. An additional SSW front symmetry indication is the satisfactory agreement between the SSW's velocity computed from these frames with the results of simulations, which assume azimuthal and axial (1D) and axial (2D) symmetries. In Fig. 5(d), we present the 2D HD simulated pressure distribution at the time when the SSW reached $r \approx 40 \mu\text{m}$, and the pressure reached $\sim 8 \times 10^9 \text{ Pa}$. The results of 1D and 2D simulations showed that the SSW TOF from this radius to the axis is $\leq 7 \text{ ns}$, which probably limits the development of HD instabilities.

In Fig. 6, one can see the light emission detected by the PMT in an explosion using Gen2 generator. The first peak ("1") seen in Fig. 6 is the light emission, produced during the wire array's explosion, which corresponds to the temporal evolution of the electrical power deposited into the array. This correlation, together with the assumption that the SSW implosion occurs when the light emission peak "3" is maximal, allows a precise measurement of the SSW's TOF. The light emission peak "2" is seen $\sim 50 \text{ ns}$ prior to the onset of 3. We consider that the increase in the light intensity seen in peak 2 is related to a transition from Fresnel to Fraunhofer diffraction pattern due to a decrease in the diameter of the converging SSW, and its falling part is related to the shrinking of the cylindrical aperture. Peak 3 is the result of light emitted from the plasma^{11,16} formed in the vicinity of the axis and has a $\sim 10 \text{ ns}$ rise time, and it decays within $\sim 20 \text{ ns}$. Peak 3 is followed by a small dip in the light intensity, which is superseded by a $\sim 230 \text{ ns}$ wide peak "4." The results of 1D HD modeling suggest that the light in peak 4 is emitted from the plasma layer expanding after

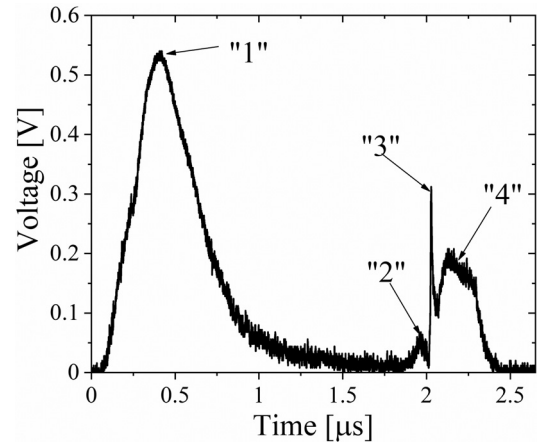


FIG. 6. Typical signal registered by the PMT during experiments on Gen2.

the SSW implosion and has a temperature of $>1 \text{ eV}$ on axis and $\sim 2000 \text{ K}$ at $r \approx 10 \mu\text{m}$. The shape of 4 is characterized by its slow intensity decrease over $\sim 200 \text{ ns}$ when the light intensity changes by $\sim 20\%$, which could be the manifestation of the two competing processes, namely, plasma cooling and expansion. The latter leads to an increase in the solid angle seen by the optical fiber.

In Fig. 7(a), we present a 400×400 pixel section from an image obtained in an explosion of the 10 mm array at Gen2 almost at the SSW implosion as estimated from the camera trigger out and PMT signals (to an accuracy of $\pm 1 \text{ ns}$). Because the light emission oversaturates the central pixels, we cannot compare intensities and cannot estimate the FWHM. However, the pattern is close to circular, indicating that the symmetry of the compressed region is most likely conserved even within $\pm 1 \text{ ns}$ with respect to the implosion. In Fig. 7(b), we present a noise-filtered image that supports this.

To summarize, cylindrical wire arrays electrical underwater explosion experiments with a deposited energy of up to 5 kJ display generally symmetrical convergence of the SSW down to $r \geq 30 \mu\text{m}$. Thus, one might expect the formation of extreme water parameters: pressure up to $\sim 10^{11} \text{ Pa}$, water density of $\sim 3 \text{ g/cm}^3$, and temperature of $\sim 1 \text{ eV}$ in the vicinity of the implosion axis using moderate pulse power generators. Images taken within $\pm 1 \text{ ns}$ from the implosion

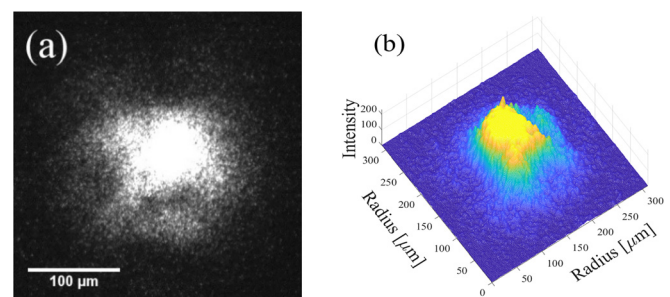


FIG. 7. (a) Magnified section of the frame obtained close to implosion; (b) 3D plot of the filtered intensity distribution of this region.

provide supplementary support to this claim. This conclusion regarding the shock symmetry is limited because of blurring of its front caused by the finite frame exposure time and experimental evidence only up to $r \geq 30 \mu\text{m}$. Hence, additional research is required regarding the shock azimuthal symmetry in the vicinity of the implosion.

We thank Dr. S. Efimov, D. Maler, and S. Gleizer for generous technical assistance and Dr. J. Leopold and Dr. S. Chefranov for fruitful discussions. This research was supported by the Israel Science Foundation Grant No. 492/18.

DATA AVAILABILITY

The data that support the findings of this study are available from the corresponding author upon reasonable request.

REFERENCES

- ¹V. E. Fortov and I. T. Iakubov, *The Physics of Non-Ideal Plasma* (World Scientific, Singapore, 1999).
- ²Y. E. Krasik, S. Efimov, D. Sheftman, A. Fedotov-Gefen, O. Antonov, D. Shafer, D. Yanuka, M. Nitishinskiy, M. Kozlov, L. Gilburd, G. Toker, S. Gleizer, E. Zvulun, V. T. Gurovich, D. Varentsov, and M. Rodionova, *IEEE Trans. Plasma Sci.* **44**, 412 (2016).
- ³A. Grinenko, V. T. Gurovich, and Y. E. Krasik, *Phys. Plasmas* **14**, 012701 (2007).
- ⁴Y. Zel'Dovich and Y. Raizer, *Physics of Shock Waves and High-Temperature Hydrodynamic Phenomena* (Courier Corporation, 2002).
- ⁵S. N. Bland, Y. E. Krasik, D. Yanuka, R. Gardner, J. Macdonald, A. Virozub, S. Efimov, S. Gleizer, and N. Chaturvedi, *Phys. Plasmas* **24**, 082702 (2017).
- ⁶D. Yanuka, A. Rososhek, S. N. Bland, and Y. E. Krasik, *Appl. Phys. Lett.* **111**, 214103 (2017).
- ⁷M. Kozlov, V. T. Gurovich, and Y. E. Krasik, *Phys. Plasmas* **20**, 112701 (2013).
- ⁸S. P. Lyon and J. D. Johnson, Report No. LA-UR-92-3407 (Los Alamos National Laboratory, 1992).
- ⁹S. G. Chefranov, *Phys. Fluids* **32**, 114103 (2020).
- ¹⁰A. Rososhek, S. Efimov, A. Virozub, D. Maler, and Y. E. Krasik, *Appl. Phys. Lett.* **115**, 074101 (2019).
- ¹¹G. Bazalitski, V. Ts Gurovich, A. Fedotov-Gefen, S. Efimov, and Y. E. Krasik, *Shock Waves* **21**, 321 (2011).
- ¹²S. Efimov, A. Fedotov, S. Gleizer, V. T. Gurovich, G. Bazalitski, and Y. E. Krasik, *Phys. Plasmas* **15**, 112703 (2008).
- ¹³B. M. Kovalchuk, A. V. Kharlov, V. B. Zorin, and A. A. Zherlitsyn, *Rev. Sci. Instrum.* **80**, 083504 (2009).
- ¹⁴A. Rososhek, S. Efimov, S. V. Tewari, D. Yanuka, K. Khishchenko, and Y. E. Krasik, *Phys. Plasmas* **25**, 062709 (2018).
- ¹⁵A. Rososhek, S. Efimov, D. Maler, A. Virozub, and Y. E. Krasik, *Appl. Phys. Lett.* **116**, 243702 (2020).
- ¹⁶D. Yanuka, A. Rososhek, S. Efimov, M. Nitishinskiy, and Y. E. Krasik, *Appl. Phys. Lett.* **109**, 244101 (2016).